NUKLEONIKA 2012;57(4):529–535

ORIGINAL PAPER

Thermal neutron radiography studies of drying of rectangular blocks of wet mortar

**Izabela M. Fijał-Kirejczyk,
Jacek J. Milczarek,
Frederick C. de Beer,
Mabuti J. Radebe,
Gabriel Nothnagel,
Joanna Żołądek-Nowak**

Abstract. The convectional drying of rectangular block of wet mortar was investigated with thermal neutron radiography technique supplemented with traditional mass and temperature measurements. The time evolution of the drying process was recorded for rectangular sample of aged mortar before and after painting its lateral sides. The receding boundary of the central core wet region was observed in the advanced stage of the process. The size, shape and water content of that region were determined for both cases of non-painted and painted sample. It was shown that in the advanced drying process the receding drying front exists irrespectively of the drying pattern observed at the early period of drying.

Key words: drying • capillary-porous media • mortar • thermal neutron radiography

I. M. Fijał-Kirejczyk✉, J. J. Milczarek,
J. Żołądek-Nowak
National Centre for Nuclear Research (NCBJ),
7 Andrzeja Sołtana Str., 05-400 Otwock/Świerk, Poland,
Tel.: +48 22 718 0060, Fax: +48 22 779 3481,
E-mail: Izabela.Fijal-Kirejczyk@ncbj.gov.pl

F. C. de Beer, M. J. Radebe, G. Nothnagel
Radiation Science,
Necsa – South African Nuclear Energy Corp. Ltd.,
Church Street West Extension, Pelindaba,
Pretoria, 0001, South Africa

Received: 1 December 2011
Accepted: 25 February 2012

Introduction

The process of drying of capillary-porous media has been studied for at least a century with standard techniques as weight and temperature measurements [2, 3, 14, 18]. The neutron radiography (NR) has been introduced into the subject of water migration within the porous media during the last decades of the 20th century [4–6, 8–13, 15–17, 20, 21]. The NR has been proved to be excellent tool for determination of the spatial water distribution inside granular capillary-porous media [10–12, 20, 21]. The main merit of this imaging technique is a high contrast between images of the dry and wet regions of the sample body [1, 7]. This advantage is due basically to very high incoherent scattering of thermal neutrons on hydrogen nuclei, which removes neutrons from the incident beam producing dark regions in the images of water containing part of the samples. In effect the drying front and its motion across the sample volume can be easily visualized and quantified from the recorded sequences of neutron radiographs.

Drying of the capillary-porous objects is a multistage process the different stages of which are conventionally distinguished by different rate of mass loss of the sample [2, 3, 18, 19]. The first period of very high rate of mass decrease has been named the constant rate period (CRP) due to almost linear dependence of the mass on time. The CRP is followed by two falling rate periods (FRP) which differ in mechanism of water transport from the sample body to the sample surface. For the

second FRP analysis, the concept of the receding drying front (RDF), separating the dry outer region from the wet central core, has been introduced and applied in analysis of the local temperature evolution over the sample [14, 19]. The drying front and its motion has been observed recently in wet quartz sand cylindrical samples with neutron radiography leaving no doubt of its existence [12].

In this work we studied the rectangular samples of a rigid capillary-porous system formed by the aged mortar designed for special constructions [5, 15]. Our aim was to investigate the drying process with particular objective of receding drying front analysis. The process was studied for the same sample first with all six boundary surfaces exposed to the drying air and then after insulating its four side walls.

Experimental

The experiments were carried out at the neutron and gamma radiography station (NGRS) at the MARIA nuclear research reactor of National Centre for Nuclear Research (NCBJ, Otwock, Poland) [4, 8, 9, 16, 21]. The drying process was observed with on-line registration of the sample mass and temperature as well as sequences of neutron radiographs for the whole process. The experimental system was essentially the same as described previously [10–12] for drying of kaolin clay and quartz sand cylinders. The sample was dried in a drying tunnel with a 60°C hot air stream flowing from above at a rate of 0.03 $m^3 \cdot s^{-1}$ (stream speed ~3 $m \cdot s^{-1}$). The sample temperature and mass were recorded every 10 s and the neutron radiographs every 2 s. Before image analysis, preprocessing procedures including the correction of pixel brightness for the black current, normalization for neutron beam flux fluctuations, as well as the median filtering were applied.

The sample was a rectangular block of 48 × 52 × 14 mm made of aged special mortar, which was saturated with water by immersion for 48 h. With the effective porosity of the mortar of ~60%, the initial mass content of water in the sample was ~29%. The same sample was investigated first with all its surfaces free and then after painting its four lateral sides with two layers of acrylic paint with the top and bottom surfaces left uncovered.

The sample was placed at a distance of ~70 mm from the detector screen on an aluminium support rod with its lower end resting on the electronic balance tray. The balance provided standard accuracy of 0.1 g. The mass of the dry sample was 34.1 g before and 35.5 g after

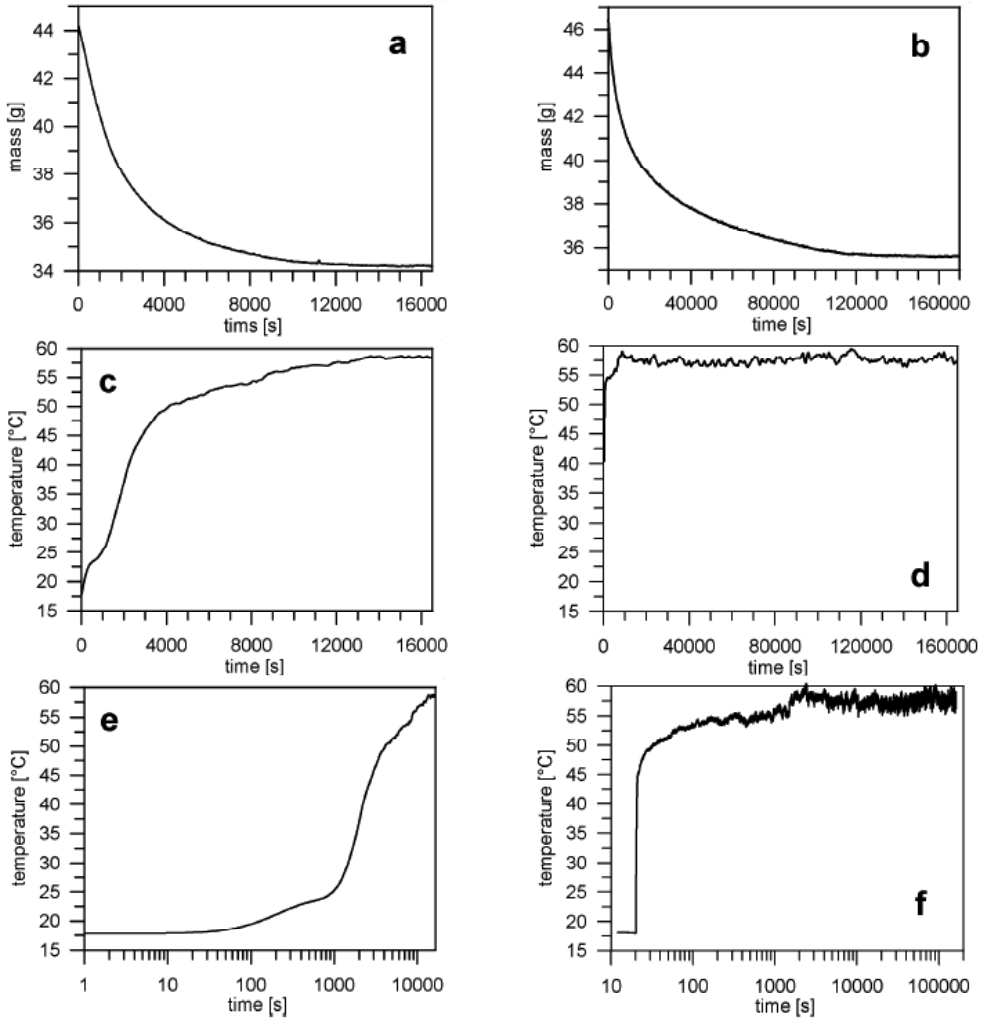

Fig. 1. The time dependence of sample mass and temperature during drying. The diagrams a, c and e correspond to the non-painted, and b, d and f to painted samples, respectively.

painting, respectively. The sample support incorporated a K-type steel sheathed thermocouple of 0.5 mm in diameter. The thermocouple penetrated the sample vertically from its lower end with thermocouple head placed at a distance of ~15 mm from the sample bottom.

Results

The sample mass decreased very fast during the first drying period, which was completed during first ~2500 s of the process for non-painted sample and ~25 000 s for the painted one (Figs. 1a and 1b). The temperature inside the non-painted sample during that period levelled off at ~25°C after fast initial increase from room temperature for the non-painted sample (Fig. 1c). No trace of such stable temperature inside the painted sample was found (Fig. 1d). At the end of that period, the water content was less than 2%. The changes in the sample mass turned unnoticeable after ~4800 s and ~48 000 s, respectively of the process (Figs. 1a and 1b). The second fast increase in the non-painted sample temperature to ~50°C was observed close to 3000 s (Figs. 1c and 1e) and afterwards the temperature was steady for the next ~1000 s until 10 000 s of the process. Then, the temperature increased to ~58°C, close to the drying air temperature. In the painted sample the change of temperature was markedly different, the increase was very steep initially until 50°C was reached. Then, a slow rise in temperature to 53°C was observed followed by an increase to 58°C at ~9000 s. The different drying periods are not as well discernible for the painted sample as for the non-painted one (Figs. 1d and 1f).

The time dependence of the water content and temperature corresponds to the changes in brightness of the neutron image of the sample. At the beginning, the sample was uniformly saturated with water (Figs. 2a and 2f). However, in the advanced period of drying the darker region separated from the sample's boundary emerged (Figs. 2b–2d, 2g–2i). That darker region was separated from the lighter layer by a discernible drying front. This drying front was moving towards the centre of the sample. For the non-painted sample the image of the wet core region was central rectangle surrounded by light grey dry sample areas. For the painted sample, the image of the dry region was of the form of a bit irregular horizontal dark strip attaining a wedge-like shape. At the end of the process, the sample image was almost uniform (Figs. 2e and 2j). One should note that the duration of the drying process is almost ten times longer for the painted than for the non-painted sample.

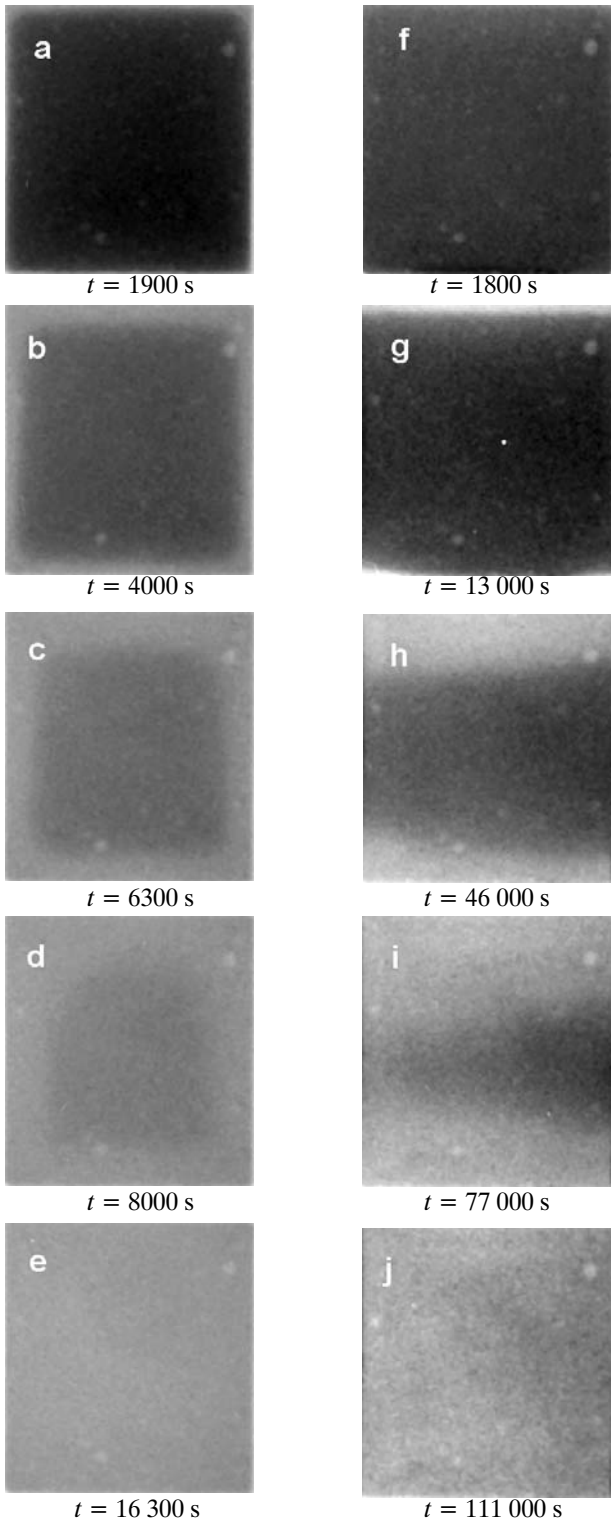

Fig. 2. The time evolution of the sample image during the advanced stages of drying. The pictures a–e present the images of non-painted samples. The pictures f–j are the images of painted samples. The evolution time is given below pictures.

Neutron image analysis

We analysed the neutron images using two different approaches. In the first approach we used statistical methods to determine the global parameters describing the sample image. In the second method the absorption of neutrons by different parts of the sample was considered.

In the stochastic analysis we treat the sample image as a stochastic matrix with elements corresponding to the image pixels and given by brightness of the pixels. The sample image was cropped from all the sequences of the recorded neutron radiographs with a simple procedure. In particular, the sample image was a matrix with 310 × 330 elements of integers from 0 to 255 (in case of 8 bit encoding of the grey level). For each sample image, the brightness histogram $H(b)$ was determined. Since in the case of discrete stochastic variable b, the $H(b)$ is the number of pixels with a given brightness b it was eas-

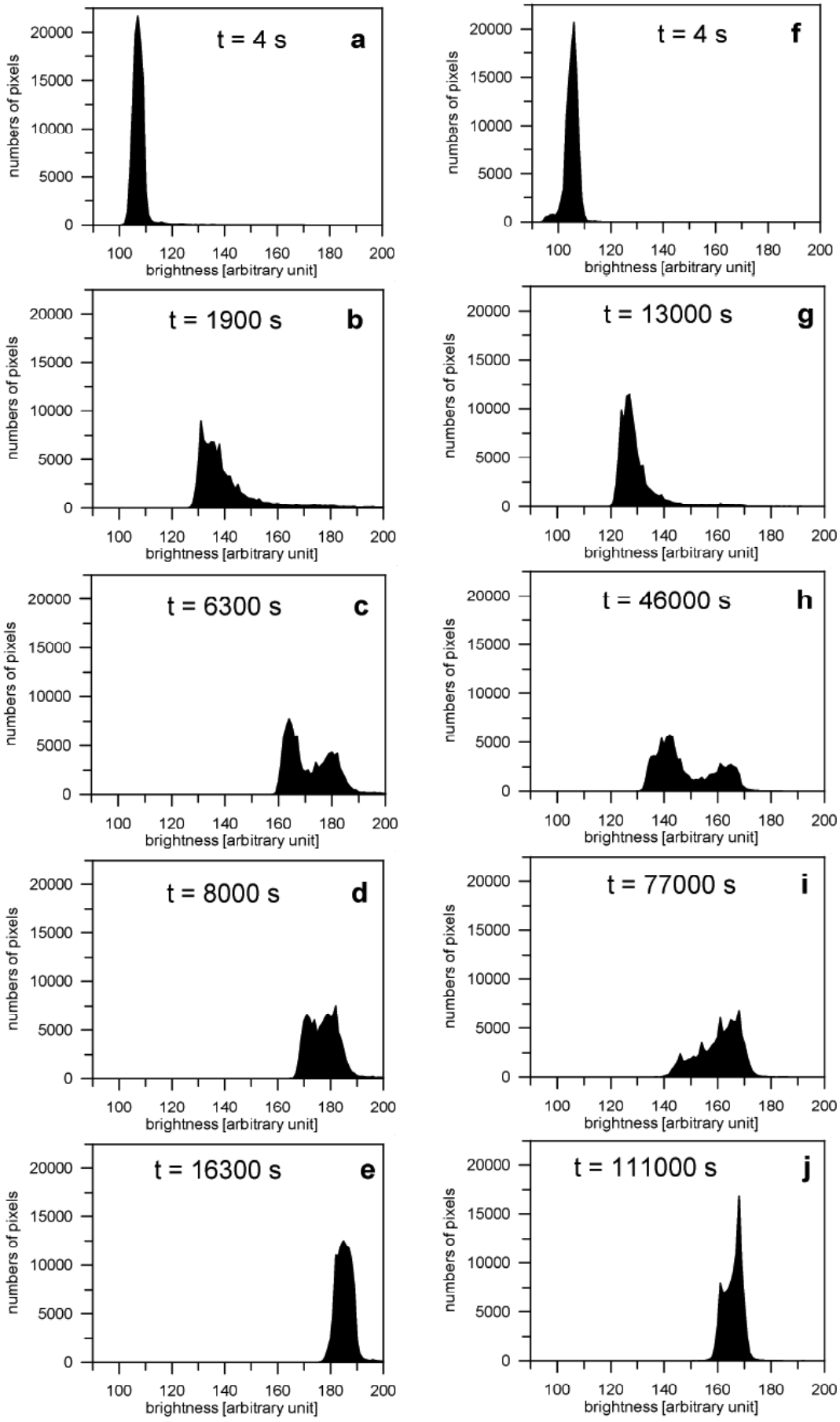

Fig. 3. The changes in grey level histograms of the sample images during drying. The histograms a–e correspond to the non-painted, and f–j to painted samples, respectively.

ily calculated with ImageJ software package. The time evolution of the image histogram revealed very profound changes in its shape during drying (Fig. 3). At the beginning, $H(b)$ consisted of a single peak corresponding to uniform image with dark grey pixels (Figs. 3a and 3f). Then, a broadening and shift of the histogram to the larger b region was observed (Figs. 3b and 3g). Further on its shape became a broad distribution with two marked maxima (Figs. 3c and 3h). At the end, the plot of $H(b)$ was close to one peak and a narrow two peaks distribution for non-painted and painted sample, respectively (Figs. 3e and 3j).

For further analysis, simple statistical parameters, the average brightness $<b>$ and brightness standard deviation Δ, were determined using the usual definitions:

$$\langle b^n \rangle = \int b^n H(b)\, db \,/ \int H(b)\, db \tag{1}$$

$$\Delta = \left(\langle b^2 \rangle - \langle b \rangle^2 \right)^{1/2} \tag{2}$$

The plot of average brightness of the sample image vs. time exhibits a fast increase at the initial period of drying (Fig. 4). The saturation of the average brightness for large times ($\sim 10^4$ s for non-painted and 10^5 s for painted sample) was found.

The standard deviation of brightness is the simplest measure of diversification of grey levels of image pixels produced by emerging patterns like the wet core region. The standard deviation plotted vs. time exhibits for the studied sample a single maximum for ~4000 s for non-painted sample and at ~40 000 s for painted one (Fig. 5).

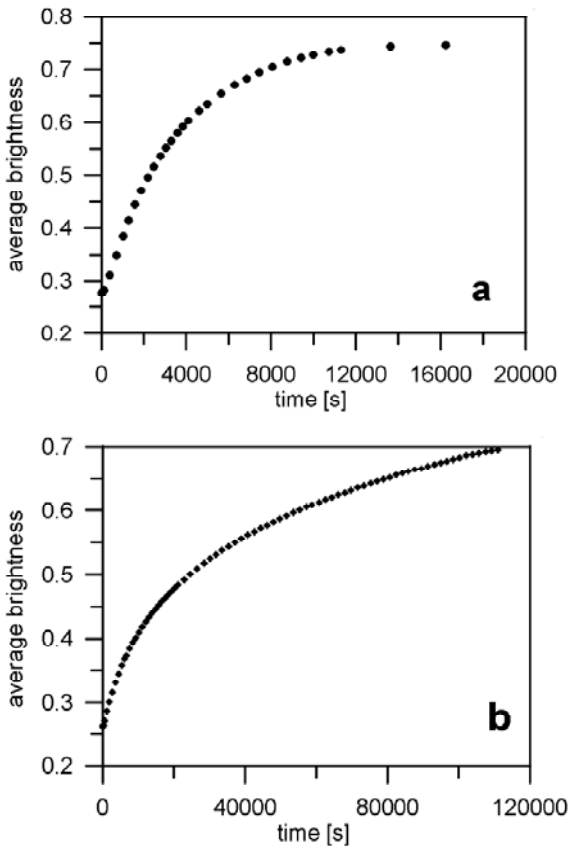

Fig. 4. The time variations of sample image brightness for the non-painted (a) and painted (b) samples.

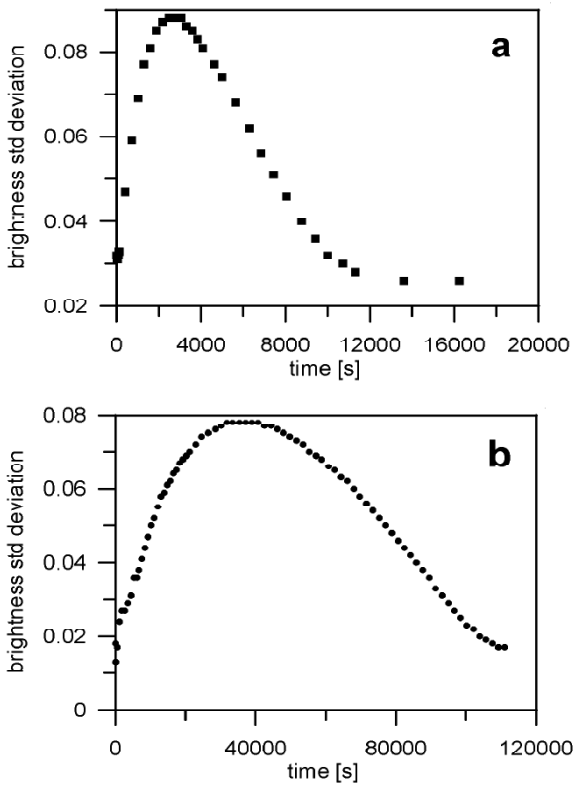

Fig. 5. The time variations of the standard deviation of the sample image brightness for the non-painted (a) and painted (b) samples.

In a standard approach [1, 6, 7, 13, 16, 17, 20] the local brightness at the point (x,y) of the imaging plane is analysed in terms of the Lambert-Beer law:

$$I(x,y) = I_0(x,y) \exp[-\Sigma(x,y) L(x,y)] \tag{3}$$

where I_0 and I are the intensities of the incident and transmitted neutrons, respectively. The parallel beam is assumed to impinge in the normal direction on the imaging plane and the neutron macroscopic cross-section Σ and the neutron path length L inside the sample are determined along the projection line meeting the (x,y) point. Since the macroscopic cross-section for water is dominated by neutron scattering, the distance from the sample to the detector plane is chosen larger than the sample width to minimize the contribution of scattered neutrons to the sample image [6, 13, 20]. That contribution is evidently smaller if L is less than the neutron mean free path Σ^{-1}.

After all image corrections (black current and image normalization) the intensity of the transmitted neutrons is proportional to the local image brightness and the macroscopic cross-section can be calculated. Here, we present the analysis performed for the vertical line plotted through the centre of the sample image. The plots of the brightness vs. the position on the line are well-like shaped (Fig. 6). The increasing brightness of the image is clearly demonstrated as decreasing depth of the brightness vs. position plots. The emerging darker region in the sample centre is observed as decreasing width of that plot. The height of that region was easily estimated (Fig. 7). It is evident that at the initial periods of drying the wet core region covers the whole sample. Then,

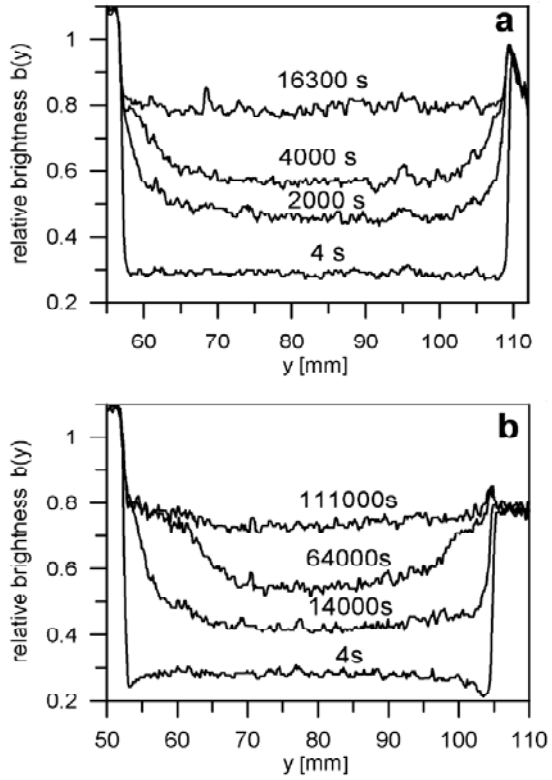

Fig. 6. The relative brightness profiles for vertical central line for the non-painted (a) and painted (b) samples. The time of the process is indicated above the corresponding plots.

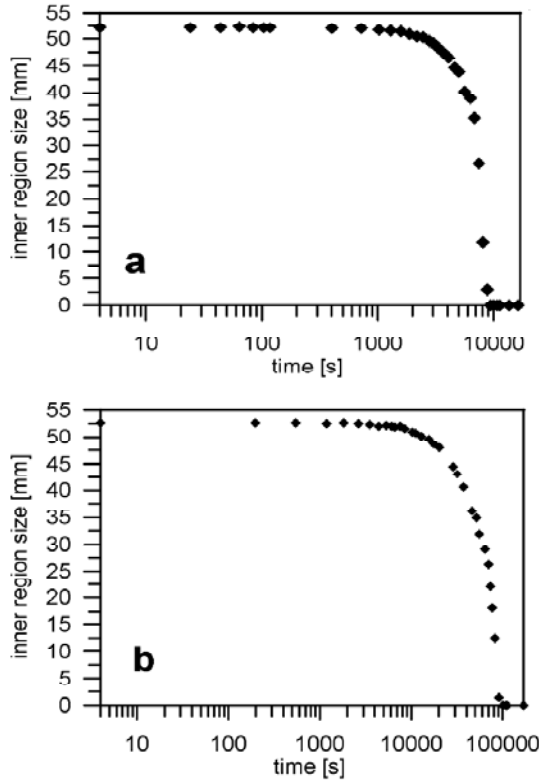

Fig. 7. The time dependence of the height of the inner wet region inside the receding drying front.

its size decreases until its ultimate disappearance. The calculated macroscopic cross-section decreases initially very steeply to reach almost steady value before a sudden drop to zero for the eventually dry sample (Fig. 8).

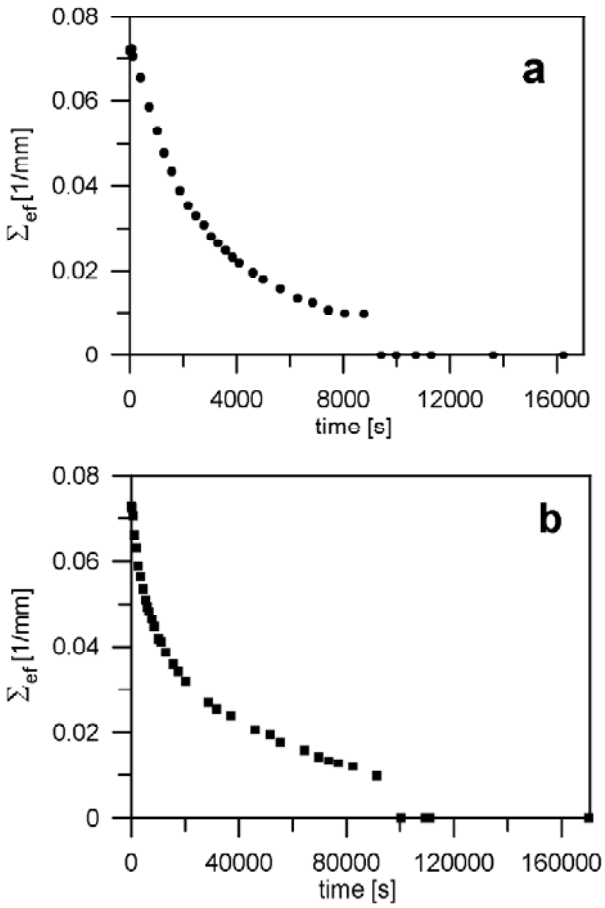

Fig. 8. The time dependence of the effective neutron macroscopic cross-section calculated for the wet inner region.

Discussion

The time dependence of the mass and temperature of the non-painted and painted samples provides no marked signs for different periods of drying process (Fig. 1). The short period of steady temperature for non-painted sample provides only a weak signature of the constant drying rate period. That feature of the rectangular sample drying is in a marked contrast to the process evolution in wet quartz sand cylinders where different phases of drying were clearly delineated with classical measurements [12]. On the other hand, the time dependence of the image global statistical parameters provide a possibility to distinguish different periods of drying for the rectangular sample. In particular, the observed maximum in the time dependence of the standard deviation of the image brightness can be used to determine the start of the last period of drying with existence of wet inner core limited by the receding drying front.

The flat spatial distribution of brightness within the sample images suggests that the scattered neutrons contribution is negligible [6, 13, 20]. This effect is due to the appropriately large sample to detector distance and the small sample thickness (14 mm) in comparison to the average neutron free path, which increases from ~15 mm, at the initial wet state, to ~100 mm at the final drying stage (Fig. 8). The effect of multiple scattering on image brightness is here less discernible than in a

rather thick (diameter of 35 mm) cylindrical specimen where the scattered neutron contribution was significant for the first drying period [10–12]. In the advanced period of drying, when the wet core begins to shrink, we can assume that the saturation of that region with water does not change and its thickness decreases similarly to its other dimensions.

Conclusions

Neutron radiography was successfully applied in the studies of drying of the rectangular block sample of aged concrete. The sample with all surfaces exposed to the drying air as well as with four sides painted was investigated. The receding drying front was unambiguously observed in both cases. The difference in drying process of the sand cylinder and mortar rectangular samples was clearly revealed.

It was demonstrated that the statistical approach to neutron image analysis yields a simple description of the drying in terms of the parameters calculated from the sample images recorded during the process. The analysis of the average brightness and its standard deviation permits to distinguish the important stages of the drying process. We confirmed that the standard image analysis permits to determine the distribution of water inside the sample. Our results support the merits of thermal neutron radiography in studies of the drying process.

Acknowledgment. This work has been supported by the Ministry of Science and Higher Education of Republic of Poland and the National Science Foundation of Republic of South Africa within the "Neutron Radiography/ Tomography of Porous Media" project no. 7963/R10/R11 performed according to the Scientific and Technological Co-operation Agreement between Poland and South Africa.

References

1. Anderson IS, McGreevy RL, Bilheux HZ (eds) (2009) Neutron imaging and applications. Springer, Berlin
2. Brosnan DA, Robinson GC (2003) Introduction to drying of ceramics. American Ceramic Society, Westerville
3. Coulson JM, Richardson JF (1956) Chemical engineering. Vol. 2. Pergamon Press, London
4. Czachor A, El-Ghany el Abd A, Milczarek JJ (2002) Determination of capillary motion of water in bricks using neutron radiography. Acta Phys Pol A 102:245–252
5. de Beer FC, Strydom WJ, Griesel EJ (2004) The drying process of concrete: a neutron radiography study. Appl Radiat Isot 61:617–623
6. Deinert MR, Parlange J-Y, Steenhuis T, Throop J, Ünlü K, Cady KB (2004) Measurement of fluid contents and wetting front profiles by real-time neutron radiography. J Hydrol 290:192–201
7. Domanus JC (ed) (1992) Practical neutron radiography. Kluwer Academic Publishers, Dordrecht
8. El-Ghany el Abd A, Czachor A, Milczarek JJ, Pogorzelski J (2005) Neutron radiography studies of water migration in construction porous materials. IEEE Trans Nucl Sci 52:299–304
9. El-Ghany el Abd A, Milczarek JJ (2004) Neutron radiography study of water absorption in porous building materials: anomalous diffusion analysis. J Phys D: Appl Phys 37:2305–2313
10. Fijał-Kirejczyk I, Milczarek JJ, Banaszak J, Trzciński A, Żołądek J (2009) Dynamic neutron radiography studies of drying of kaolin clay cylinders. Nukleonika 54:123–128
11. Fijał-Kirejczyk IM, Milczarek JJ, Banaszak J, Żołądek J, Trzciński A (2010) Drying of kaolin clay cylinders: dynamic neutron radiography studies. Defects and Diffusion Forum 297/301:508–512
12. Fijał-Kirejczyk IM, Milczarek JJ, Żołądek-Nowak J (2011) Neutron radiography observations of inner wet region in drying of quartz sand cylinder. Nucl Instrum Methods A 651:201–210
13. Lehmann EH, Vontobel P, Kardjilov N (2004) Hydrogen distribution measurements by neutrons. Appl Radiat Isot 61:503–509
14. Luikov AV (1975) Systems of differential equations of heat and mass transfer in capillary-porous bodies (Review). Int J Heat Mass Transfer 18:1–14
15. McGlimm PJ, de Beer FC, Aldridge LP *et al*. (2010) Appraisal of a cementitious material for waste disposal: Neutron imaging studies of pore structure and sorptivity. Cement Concrete Res 40:1320–1326
16. Milczarek JJ, Czachor A, El-Ghany el Abd A, Wiśniewski Z (2005) Dynamic neutron radiography observations of water migration in porous media. Nucl Instrum Methods A 542:232–236
17. Pleinert H, Sadouki H, Wittmann FH (1998) Determination of moisture distributions in porous building materials by neutron transmission analysis. Mater Struct 31:218–224
18. Scherer GW (1990) Theory of drying. J Am Ceram Soc 73:3–14
19. Schlünder EU (2004) Drying of porous material during the constant and the falling rate period: a critical review of existing hypotheses. Drying Technol 22:1517–1532
20. Shokri N, Lehmann P, Vontobel P, Or D (2008) Drying front and water content dynamics during evaporation from sand delineated by neutron radiography. Water Resour Res 44:W06418 1–11
21. Żołądek J, Milczarek JJ, Fijał-Kirejczyk I (2008) Dynamic neutron radiography studies of water migration in beds of natural zeolite. Nukleonika 53;Suppl 2:S113–S119